COMSOL CONFERENCE 2023 MUNICH

Modeling of a vapor chamber using Comsol Multiphysics®

M. Rodriguez[1], B. Chiné[2]
School of Materials Science and Engineering, Costa Rica Institute of Technology, Cartago, Costa Rica
P.O. Box 159-7050, Cartago, Costa Rica, [1]melirova11@gmail.com, [2]bchine@itcr.ac.cr

Abstract

High power consumption chips have already become a major challenge for modern processors causing low thermal performances. Existing thermal solutions are not able to solve these high temperature issues efficiently. Two-phase cooling devices such as heat pipes and vapor chambers have proven to be among the most efficient active thermal solutions for electronics cooling.

In this work, we model in COMSOL Multiphysics® 6.0 a small 3D vapor chamber used as a thermal solution for cooling microprocessors in laptops. We set up the computational frame by resorting to the heat pipe model of the Application Library. The steady state equations of conservation of fluid mechanics and heat transfer are implemented by using the Laminar Flow, Brinkmann Equations and Heat Transfer in Porous Media interfaces and the multiphysics couplings already available in the software. The computational model takes full advantage of both CFD Module and Heat Transfer Module, where these interfaces are located, and of thermodynamic calculations for the vapor-liquid system using the Chemical Reaction Engineering Module.

The computational model is able to simulate the heat transfer process from the evaporator zone to the condenser at steady state. The results are validated with a real vapor chamber previously tested in a thermal laboratory from a third-party. The fit between the model and the experimental data reaches close to 0.34% error in predicting the transistor layer's maximum temperature, 2% error in predicting the temperature on the top surface of the chamber, and about 4% error in computing the heat exchanger area.

Although we use a single input power and a fixed geometry, the model is useful to analyze real vapor chamber in case of changes in the properties of materials, working fluid or percentage of porosity of the wick medium, as long as the dimensions or proportions of its parts are not altered.

Keywords: Thermal solution, CFD, heat exchanger, Brinkmann equations, heat transfer in porous media.

1. Introduction

Currently, the simplest and most common way to achieve the cooling of a microprocessor is by using heat pipes, however, there are other thermal solutions called vapor chambers, which can dissipate heat more efficiently. Nevertheless, these vapor chambers tend to be reserved for premium and higher power segments, so there's less information about their operation.

Vapor chambers are thermal solutions that use both, boiling and condensing processes to maximize heat transfer in order to cool down electronic microchips. As heat is applied to one side of the vapor chamber, the fluid near the heat source (the chip) reaches its boiling temperature and vaporizes. The vapor then travels to the other side of the vapor chamber, where the heat exchanger is located, and condenses into a liquid. The condensed fluid returns to the hot side by gravity or capillary action, ready to vaporize again and repeat the cycle [1,2].

The main difference between a heat pipe and a vapor chamber is the distance the liquid and vapor must travel, and the way the liquid is transported back from the condenser to the evaporator. In a two-phase heat pipe, the liquid evaporates at one end of the pipe, passing through its entire length, and then condenses at the opposite end of the pipe [1,2]. Whereas in a vapor chamber, heat is applied at the bottom of the chamber where the liquid evaporates, travels a relatively short distance and condenses on the top plate of the vapor chamber.

Vapor chambers are used as a heat sink for high heat flux cooling applications due to their low resistance and uniformity. In addition, vapor chambers are preferable over heat pipes for electronic cooling with heat fluxes greater than 50 W/cm^2, since the heat flux has a two-dimensional or three-dimensional pattern, compared to the one-dimensionality in conventional heat pipes [3].

2. Model description

2.1. Physical model

For the generation of the model, a geometry of three-dimensional blocks was built. The assembly of blocks forms the multiple layers of different materials that make up the vapor chamber (Table 1).

Due to computational restrictions, it was decided to generate a less complicated version of the model, with a simpler geometry where the shape of the vapor chamber was reduced to only its central body, with smaller dimensions of 10x19 mm to reduce the number of degrees of freedom of the model. Therefore, Fig. 1 shows the simplified geometry that was used for the simulation of the vapor chamber.

It is important to highlight that the vapor chamber has a symmetrical geometry in the y-z plane, and that the heat transfer behavior is also

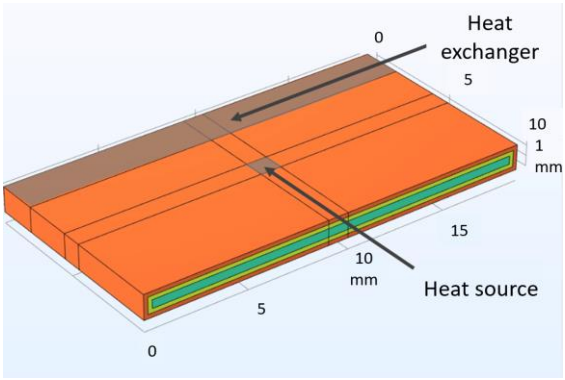

Figure 1. Original dimentions of vapor chamber body.

expected to be symmetrical, therefore, it was decided to reduce the geometry of the object by half to have computational requirements. Fig. 2 shows the final shape of the chamber.

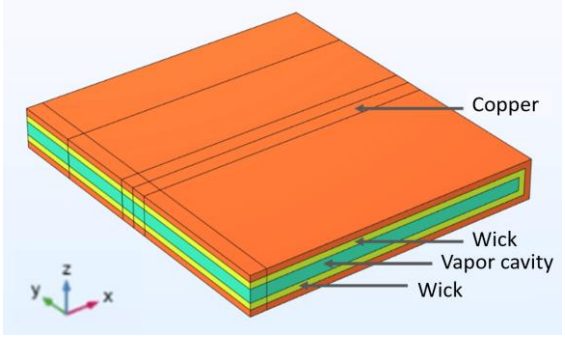

Figure 2. Simplified vapor chamber and its layers.

Table 1. Specifications of vapor chamber layers

Quantity	Name	Material	Thickness (mm)
2	Copper	Copper solid	0.2
2	Wick	Copper 68% porosity	0.2
1	Cavity	Water	0.4

From Figs. 1 and 2, it should be noted that the heat exchangers underwent a modification, since real heat exchangers usually have very thin and tall sheets called fins, which help to increase the surface area of the copper and thus increase its heat transfer capacity. However, building these fins in the model would imply a considerable increase in the number of elements to be solved, and therefore, would also increase the processing time unnecessarily. To compensate for the absence of the fins, a work plane and a domain partition feature were placed on the wing of the vapor chamber to delimit the space in which the heat exchanger is located, and on the surface of that region, an edge condition was established where a heat transfer coefficient was assigned, which was obtained from a full factorial design of experiment, which basically was an iterative process of multiple runs until finding a coefficient that gave temperature results similar to those reported in the experimental data from a third party laboratory.

Another important aspect regarding the construction of the model is that a domain partition function was also used in the lower part of the vapor chamber as a heat source, to be able to select only the 1 x 1 mm surface as heat generator, which would normally correspond to the CPU.

2.2. Mathematical description

The steady state equations of conservation of fluid mechanics and heat transfer are implemented by using the Laminar Flow, Brinkmann Equations and Heat Transfer in Porous Media interfaces and the multiphysics couplings already available in the software. The computational model takes full advantage of both CFD Module [4] and Heat Transfer Module [5], where these interfaces are located, and of thermodynamic calculations for the vapor-liquid system using the Chemical Reaction Engineering Module [6].

The steady state governing energy conservation, both for solid and fluid domain, is defined as the following [5]:

$$\rho Cp\mathbf{u} \cdot \nabla T + \nabla \cdot \mathbf{q} = Q \qquad (1)$$

where ρ is the density of the material (kg/m^3), Cp means the specific heat capacity (J/(kg K)), $\mathbf{u}$ (m/s) is the velocity field in a fluid domain, T (K) is the temperature, $\mathbf{q}$ corresponds to the heat flux (W/m^2), and Q is the heat source (W/m^3). In addition, the first term on the left side of the equation represents the convective term of heat transfer in a fluid region, while the second term corresponds to the diffusive term.

Regarding the properties of the fluid in the vapor cavity, it is assumed that the transport of the working liquid will be given by laminar flow, then the conservation of momentum can be modeled using the Navier-Stokes equation for compressible fluids, which is displayed as [4]:

$$\nabla \cdot (\rho\mathbf{u}) = 0 \qquad (2)$$

$$\rho(\mathbf{u} \cdot \nabla)\mathbf{u} = \nabla \cdot \left[-p\mathbf{I} + \mu\left[\nabla\mathbf{u} + \{\nabla\mathbf{u}\}^{T}\right] - \frac{2}{3}\mu[\nabla \cdot \mathbf{u}]\mathbf{I} + \mathbf{F}\right. \qquad (3)$$

where p (Pa) is the pressure, μ is the viscosity (Pa.s), $\mathbf{I}$ is the identity tensor, and $\mathbf{F}$ means the volumetric external forces applied to the fluid (N/m^3).

Furthermore, for the porous wick domain we used the Brinkman equations to compute fluid velocity and pressure fields of single-phase flow in the laminar flow regime [4,6]. Brickman equation is an extension to Darcy's law that includes a term that accounts for the viscous transport in the momentum balance. If ε is the porosity, κ (m^2) the permeability, and Q_m (kg/(m^3 ·s) a mass source or sink, we have the following differential equation for the conservation of the linear momentum:

$$\frac{\rho}{\varepsilon}(\mathbf{u}\cdot\nabla)\frac{\mathbf{u}}{\boldsymbol{\varepsilon}} = \nabla\cdot[-p\mathbf{I} + \frac{\mu}{\varepsilon}[\nabla\mathbf{u} + \{\nabla\mathbf{u}\}^{\mathrm{T}}] - \frac{2}{3}\frac{\mu}{\varepsilon}[\nabla\cdot\mathbf{u}]\mathbf{I} - \left(\kappa^{-1}\mu + \frac{Q_m}{\varepsilon^2}\right)\mathbf{u} + \mathbf{F} \quad (4)$$

Regarding the energy conservation, the thermal conductivity can be cleared from Fourier's Law:

$$\mathbf{q} = -k\cdot\nabla T \quad (5)$$

where $\mathbf{q}$ is the former heat flux density vector, k is the conductivity of the material (W.m^{-1}. K^{-1}), and ∇T is the temperature gradient (K.m^{-1}). However, in this case the effects of the porous medium must also be considered through the effective thermal conductivity in such a way that:

$$\mathbf{q} = -keff\cdot\nabla T \quad (6)$$

The effective thermal conductivity *keff* varies depending on the porosity of the porous material and the conductivity of the fluid, and is calculated from the theoretical model of Halpin-Tsai [7]:

$$keff = \frac{1+\eta(1-\varepsilon)}{1-\eta(1-\varepsilon)} \quad (7)$$

$$\eta = \frac{\frac{k_d}{k_c}-1}{\frac{k_d}{k_c}+1} \quad (8)$$

In these equations $\boldsymbol{\varepsilon}$ is the porosity of the wick structure (% in fractional notation), k_d is the thermal conductivity of the discrete phase (W.m^{-1}. K^{-1}) and k_c represents the thermal conductivity of the continuous phase (W.m^{-1}. K^{-1}).

2.3. Boundary conditions

The boundary conditions, and the thermodynamic relationships used in this work, are developed following the heat pipe model, available in the Application Library of COMSOL Multiphysics® 6.0 [6].

For the laminar flow, at the cavity-wick interface we prescribe the pressure to equal the saturated vapor pressure of water, as a function of temperature. No slip conditions are applied on the walls of the vapor cavity.

For the porous flow in the copper wick, at the cavity-wick interface the velocity is computed from the vapor flow rate on the cavity side. Again, no slip boundary conditions are used on the walls. A pressure point constraint is set on the solid wall of the wick.

Regarding the energy balance in the vapor chamber, we set the heat source, a convective heat flux leaving the chamber by defining an appropriate heat transfer coefficient, and a boundary heat source on the inner wick surface to account for the heat associated with the phase change of water.

Finally, the multiphysics couplings of the computational model take full advantage of both CFD Module and Heat Transfer Module, well relating flow and heat transfer.

2.4. Mesh parameters

The meshing strategy employed in this study uses a free quadrilateral mesh, which generates square partitions on an initial surface within the vapor chamber. The maximum element size at all nodes is set to 0.1 mm, which is 0.5 times the thinnest object thickness. In addition, a boundary layer function is incorporated. This boundary layer within the mesh creates a dense distribution of elements in the normal direction along the interface between the vapor cavity and the porous material. Finally, a sweeping function is applied to ensure that the newly defined mesh on the origin face is distributed along the vapor chamber, as depicted in Fig. 3. The final computational domain has nearly 10^7 free quads elements and a final average element quality of 0.99.

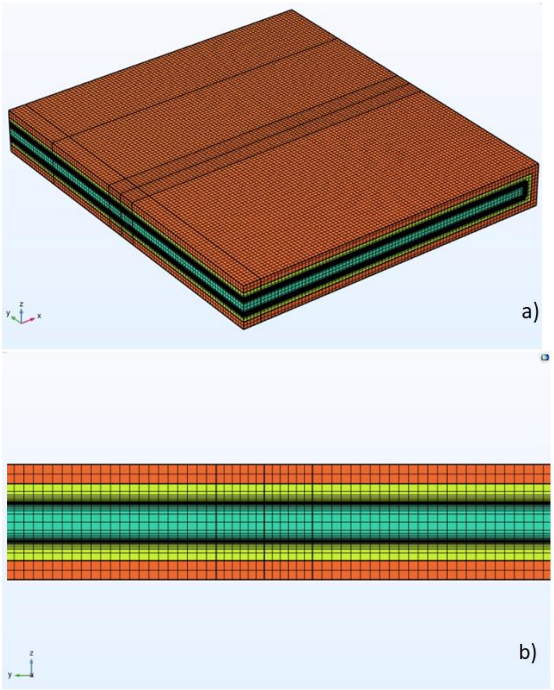

Figure 3. Meshing of the model: a) Isometric view and b) Cross section of the chamber.

3. Results and discussion

The resulting system of partial differential equations was numerically solved with COMSOL Multiphysics® 6.0.

In order to make sure the computational results were accurate, these were compared to measurements from a trusted third party's thermal laboratory. However, due to confidentiality agreements with that third party, all magnitudes displayed in the results are shown as normalized

values.

Following the optimization of power values and heat transfer coefficients based on a full factorial design of experiments, the model successfully converged displaying the results shown in Fig. 4.

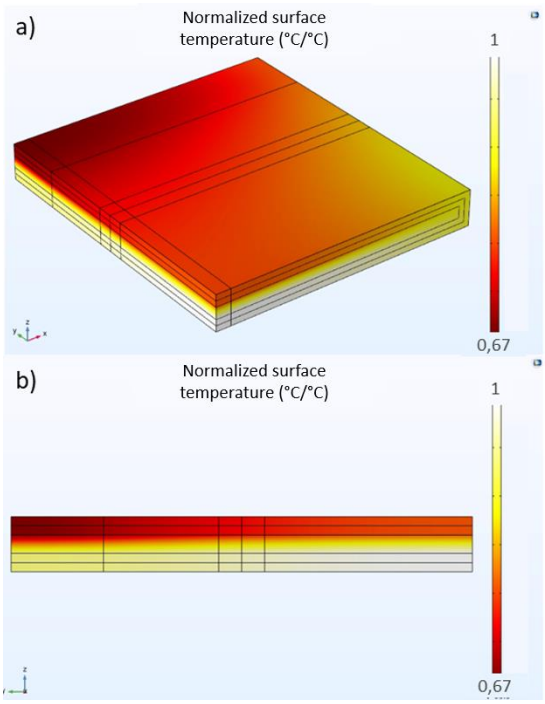

Figure 4. Temperature contours on the external surface of the vapor chamber: a) Isometric view and b) Cross-sectional view in the center of the chamber.

As indicated by the color scale for temperature on the right side of the image, the hottest regions (white) correspond to the lower base of the chamber and the center, precisely where the heat source is located and where the working fluid evaporates within the chamber. Meanwhile, the less heated contours (red) are found over the heat exchanger back inside the vapor chamber.

The following Fig. 5 shows the points of interest where the temperature was measured in the model, which also matches with the same location of the thermocouple's placement in the laboratory for the real system.

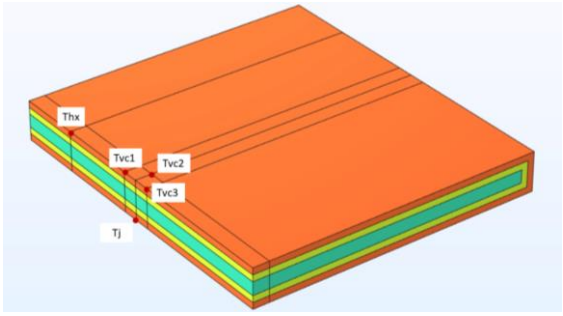

Figure 5. Position of temperature measurement points in the vapor chamber.

In Fig. 5 Tj corresponds to the temperature at the transistor layer, caused by the heat source. Essentially, it refers to the temperature at the base of the steam chamber, in the center of the heat source. Tvc is the average of temperatures Tvc1, Tvc2, and Tvc3, around the heat source, on the upper surface of the vapor chamber. Finally, Thx corresponds to the temperature at the edge of the heat exchanger, right in the center.

Table 2 gives the comparison between the temperatures of the model and the laboratory results, using a power input of 0.0533 W/W and a heat transfer coefficient of 9.75 (W/m2K)/(W/m2K) for the heat exchanger.

Table 2. Percentage of error of the different temperatures of the model with respect to the experimental results.

Temperature	Model	Laboratory	%error
Tj (°C/°C)	1.00	1.00	0.34
Tvc (°C/°C)	0.98	1.00	2.17
Thx (°C/°C)	0.96	1.00	3.70

Considering that the thermal circuit from the source region to the exterior has multiple thermal resistances as shown in Fig. 6, another way to check the model accuracy is comparing its results versus the experimental data, by calculating the thermal delta of two temperature points that are part of a thermal resistance inside the thermal circuit. The quantified error between the thermal deltas of the model and the laboratory are given in Table 3.

Figure 6. Thermal circuit from the transistor layer to room temperature.

Table 3. Percentage of error between the thermal deltas of the model and the experimental results.

Temperature	Model	Laboratory	%error
Δ j-vc (°C/°C)	1.09	1.00	9.24
Δ vc-hx (°C/°C)	0.15	1.00	84.54
Δ hx-a (°C/°C)	1.06	1.00	6.01

From the former tables, it can be observed that the model achieved a temperature in the transistor layer (Tj) practically identical to that of the vapor chamber examined in the laboratory, resulting in an error percentage of 0.34% compared to experimental data. Similarly, the error percentage for temperatures Tvc and Thx was also minimized.

Furthermore, the model successfully mimicked a behavior like the chamber examined in the laboratory in terms of temperature gradients. The largest temperature difference was between Tj and Tvc, indicating good heat transfer from the heat source to the vapor chamber, which ultimately is the thermal solution's objective: dissipating heat from the microprocessor or heat source. The smallest

temperature difference was between Tvc and Thx, indicating a good fit of the model as it imitates the functionality of the vapor chamber in maintaining an almost constant temperature across its upper surface.

This suggests that the working fluid is fulfilling its evaporation-condensation cycle by circulating through the porous material inside the chamber. Additionally, Fig. 7 illustrates the final effective thermal conductivity found by the model at the interface between the porous medium and the vapor cavity. This effective thermal conductivity has an average value of 64.02 W/mK, considering the high thermal conductivity of the copper in the porous material with a 68% porosity, and the low thermal conductivity of water in its liquid state.

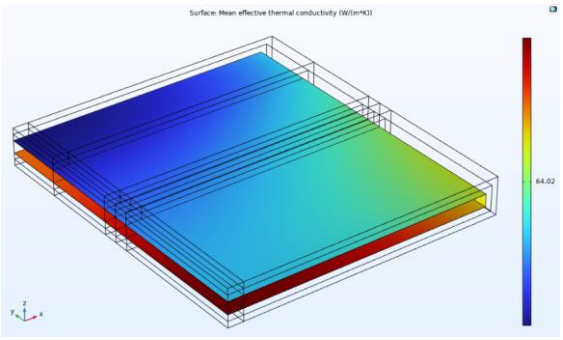

Figure 7. Average effective thermal conductivity at the vapor cavity-porous material interface.

These results demonstrate that, with a power of 0.0533 W/W and a heat transfer coefficient of 9.75 (W/m2K)/(W/m2K), the model reasonably replicates the temperature outcomes of the actual vapor chamber at its most relevant measurement points. However, being a simplified and scaled-down model, it is constrained from undergoing alterations in its geometry, as this would render the power and heat transfer coefficient values invalid. Consequently, a new series of simulations would be required to reestablish correlation with the laboratory experimental data.

Nevertheless, even though the model cannot provide insights into the behavior of the vapor chamber under scenarios of variable power, the results remain a valuable resource for qualitatively understanding how the real vapor chamber dissipates heat from the heat source to its cooler ends. Furthermore, as long as the geometry or proportions of the chamber remain unchanged, the model continues to offer a reliable response regarding the expected temperature values Tj and Tvc if properties of the components were to be altered, such as the chamber material, working fluid composition, or porosity percentage of the porous medium within the chamber.

Conclusions

This study developed a scaled-down model of a vapor chamber with simplified geometry compared to the reference real-world chamber. The model accurately simulates heat transfer from the heat source to the liquid condensation area in the heat exchanger. It demonstrates impressive fidelity to experimental data, exhibiting less than 1% error in reporting critical temperature values in the source region. Additionally, the model can provide temperature values at the upper surface of the chamber and in the heat exchanger, with errors of 2% and 4% respectively. However, the model's applicability is contingent on maintaining fixed geometry and specific normalized input parameters. Due to its scale, caution is advised in extrapolating results for real-world applications with higher power inputs.

References

[1] T.P. Cotter, “Theory of heat pipes”, *Report LA-3246-MS*, Los Alamos Scientific Laboratory, Los Alamos, New Mexico (USA), 1965.

[2] U. Vadakkan, S. V. Garimella, and J. Y. Murthy, “Transport in flat heat pipes at high heat fluxes from multiple discrete sources,” *J. Heat Transfer*, vol. 126, no. 3, pp. 347–354, 2004.

[3] M. Bulut, S. G. Kandlikar, and N. Sozbir, “A Review of Vapor Chambers,” *Heat Transf. Eng.*, vol. 40, no. 19, pp. 1551–1573, 2019.

[4] CFD Module, *User’s Guide*, Version 6.0, 2021.

[5] Heat Transfer Module, *User’s Guide*, Version 6.0, 2021.

[6] Chemical Reaction Engineering Module, *User’s Guide*, Version 6.0, 2021.

[7] L. Voisin, Viviana Pavez, and K. Pavez, “*Fenómenos de Transporte en Metalurgia Extractiva*,” Univ. Chile Aux. Exequiel Marambio, pp. 1–14, 2011.

Acknowledgements

The authors gratefully acknowledge the technical guidance provided by the thermal engineer Victor Jimenez for his inputs on modeling thermal solutions and the *Vicerrectoria de Docencia* of the Costa Rica Institute of Technology.